Journal of Zhejiang University-SCIENCE A (Applied Physics & Engineering)
ISSN 1673-565X (Print); ISSN 1862-1775 (Online)
www.zju.edu.cn/jzus; www.springerlink.com
E-mail: jzus@zju.edu.cn

Numerical investigation of the influence of companion drops on drop-on-demand ink jetting*

Hai-yun ZHANG†, Jin WANG†‡, Guo-dong LU

(*Institution of Engineering and Computer Graphics, Zhejiang University, Hangzhou 310027, China*)

†E-mail: gray_sun@zju.edu.cn; dwjcom@zju.edu.cn

Received Feb. 21, 2012; Revision accepted July 9, 2012; Crosschecked July 11, 2012

Abstract: In this study we characterized and investigated the specific phenomenon of "companion drops" in the drop-on-demand (DOD) ink jetting process. A series of simulations based on a piezoelectric DOD printhead system is presented, adapting the volume-of-fluid (VOF) interface-capturing method to track the boundary evolution and model the interfacial physics. The results illustrate the causality between the generation of companion drops and droplet deviation behavior, as well as their close correlations with ink jetting straightness and printing accuracy. The characteristics of companion drops are summarized and compared with those of satellite drops. Also, a theoretical mechanism for the generation of companion drops is presented, and their effects and behaviors are analyzed and discussed. Finally, the effects of critical factors on the generation of companion drops are investigated and characterized based on variations in the printable pressure range. Recommendations are given for the suppression of companion drops and for the improvement of printing accuracy.

Key words: Drop-on-demand (DOD) ink jetting, Droplet deviation, Companion drops, Computational fluid dynamics (CFD), Volume-of-fluid (VOF) method

doi:10.1631/jzus.A1200045 **Document code:** A **CLC number:** O35

1 Introduction

Drop-on-demand (DOD) inkjet printing technology, serving as a useful method to eject a controlled quantity of material to a specific location, has been increasingly applied in various applications, ranging from conventional graphic printing to new areas, such as fabrication of integrated circuits (ICs), light-emitting diodes (LEDs), rapid prototyping (RP), micro-electro-mechanical systems (MEMSs), cell printing and drug delivery. A schematic presentation of a typical piezoelectric DOD ink jetting system is shown in Fig. 1. The piezo printhead is the kernel component of a DOD ink jetting system, and consists of an ink chamber connected to a piezoelectric actuator that can be excited by an electrical signal pulse (Eslamian and Ashgriz, 2011). The end of the chamber is built as a convergent jetting nozzle. When a voltage pulse is applied to the actuator, the piezoelectric material alters its dimensions periodically and compresses the ink in contact with the actuator, generating a sudden pressure perturbance and ultimately leading to the ejection of an ink drop from the nozzle. The chamber is then refilled with ink from an ink reservoir.

Printing precision or accuracy is an inherent demand for DOD ink jetting, and is a complex issue involving multiple factors that can be divided into three different categories: jetting performance, equipment dynamics and mechanics, and ink-substrate interaction. Precision ink jet printing relies strongly on the accuracy and uniformity of the droplet generation process (Dijksman *et al*., 2007), which can be expressed by the drop velocity and distribution

‡ Corresponding author

* Project supported by the National Key Technology R&D Program (No. 2011BAD01B03), the Key Project of Science and Technology Program of Zhejiang Province (No. 2009C11099), and the Zhejiang Provincial Natural Science Foundation (No. Y1110230), China

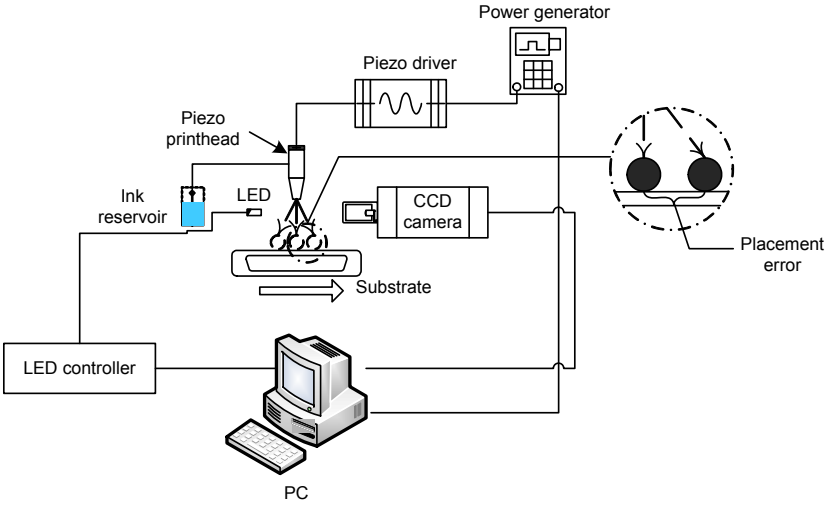

Fig. 1 Schematic illustration of a piezoelectric inkjet nozzle system

towards the target and perpendicular to the direction of the flow. Due to the relative motion of the printing substrate in front of the printhead, the larger is the distribution, the greater will be the placement error made on the medium. The jetting and droplet formation process can be observed using optical charge-coupled device (CCD) cameras (Fig. 1). Fig. 2 shows a representative image sequence of a droplet formation process (Jang *et al*., 2009).

During the droplet formation process, two phenomena occur that significantly jeopardize the jetting accuracy: satellite drops and ligaments and droplet deviation. Satellite drops can easily change the drop velocity towards the target, thus distorting the droplet flight time and printing pattern as the printhead or substrate is moving. Droplet deviation, as the ejected drop flies off the central axis and drifts perpendicular to the direction of the flow, directly changes jetting directionality and straightness. Both phenomena result in undesirable placement errors and printing inaccuracy. Thus, for the purpose of improving printing accuracy, an exhaustive study of both phenomena is of great significance.

Several investigations on satellite drops and ligaments, including their behaviors and the conditions under which they are created, have been carried out (Notz *et al*., 2001; Hoath *et al*., 2009). Recently, Dong and Carr (2006) investigated the effect of the liquid and system parameters on the recombination of the primary drop and satellites. Kwon (2010) used the measured DOD drop formation curve and the instantaneous jetting speed curve to understand the

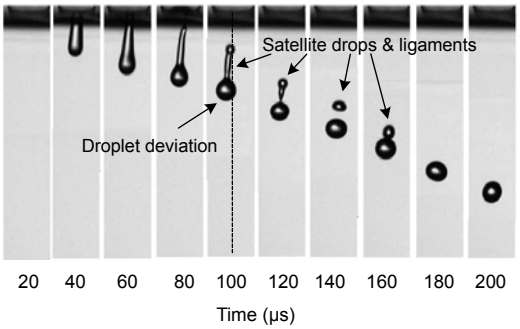

Fig. 2 A representative image sequence of DOD inkjet drop formation (Jang *et al*., 2009)

waveform effects on satellite drops and ligaments. While there have been numerous attempts to understand the formation and behavior of satellite drops, to our knowledge, an investigation of the droplet deviation phenomenon is still lacking. To date, little has been published about the droplet deviation phenomenon, which is as significant as satellite drops to jetting performance and printing quality.

As a consequence of the evolution of numerical methods and increased computing power, computational fluid dynamics (CFD) has become a promising tool to understand the jetting behavior and overcome the limitations of theoretical models. Among diverse approaches, the volume-of-fluid (VOF) method has proved effective and successful for its simplicity and robustness (Moon *et al*., 2008; Link and Semiat, 2009). Wu *et al*. (2004) demonstrated the feasibility of reproducing the full cycle of the ink-jet printing process including drop ejection, drop formation and drop collision against a target substrate by developing

an axisymmetric 3D simulation system, using the VOF method combined with a continuum-surface-force (CSF) model. Anantharamaiah *et al*. (2007) employed the CFD code from Fluent Inc. to investigate the relationship between the nozzle inlet roundness and the diameter of an ejected liquid jet in the applications of hydro-entangling. Although other numerical methods have been proposed (Yu *et al*., 2005; Suh and Son, 2008), the VOF methods are still considered the usual methods to model drop formation in DOD ink-jet printheads.

In this paper, we aim to understand droplet deviation behavior in the ink jetting and droplet formation process to ultimately suppress their undesirable effects and minimize placement errors. The rest of the paper is organized as follows: Section 2 provides a description of the jetting system setup and numerical simulation based on the VOF method. Section 3 summarizes a series of jetting simulations, characterizes the phenomenon of "companion drops", reveals its correlation with droplet deviation and discusses its features in comparison with satellite drops. Section 4 presents the theoretical mechanism of companion drop generation, and discusses their effects and behaviors. In Section 5, the effects of factors related to the formation of companion drops are investigated and characterized in terms of printable range. Finally, concluding remarks of this paper are summarized in Section 6.

2 Ink jetting simulation

2.1 Jetting system setup

To investigate droplet deviation behavior, we adopted an axisymmetric 3D model of a piezoelectric inkjet printhead. The physical phenomena in the piezoelectric printhead are very complicated due to the combination of piezoelectricity, elasticity and multiphase fluid dynamics (Wijshoff, 2010). To simplify the problem and focus on the process of droplet ejection, the printhead is modeled as a straight tubular chamber with a flat-plate piezoelectric material and ending in a convergent nozzle. The computational domain considered here consists of only part of the chamber, the nozzle of specific dimensions and the outer region through which the droplet travels (Fig. 3). The ink chamber radius was 80 μm, the total length of the ink chamber was 600 μm, the tapered nozzle region had a length of 400 μm, the orifice radius was 30 μm, and the air column had a radius of 150 μm and a length of 1500 μm. The wall that enclosed the liquid solution inside the chamber was specified as a wall boundary condition with no slip and had 90° contact angles.

The ink jetting process is activated by an electrical pulse, which turns into a pressure wave after activating the piezoelectric material, as previously described. Recent studies have gradually revealed a correlation between the given electrical pulses and the

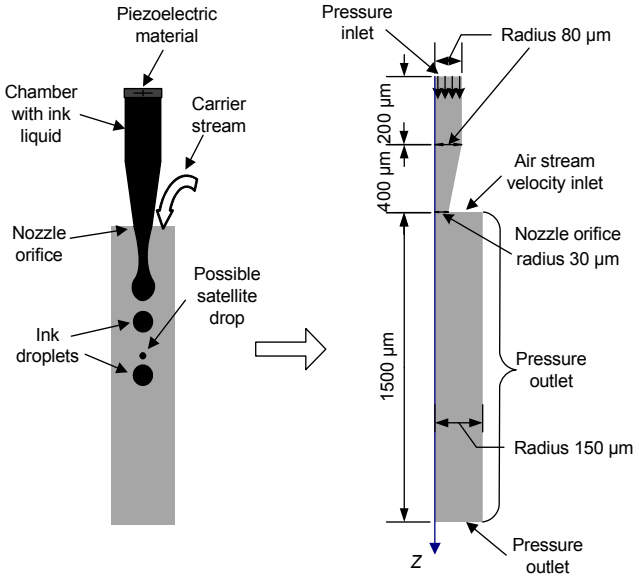

Fig. 3 Schematic of an inkjet printhead and the computational setup

resulting pressure generated inside the nozzle (Goghari and Chandra, 2007; Cibis and Krüger, 2008). In the proposed ink jetting system, the excitation pressure was employed as a pressure boundary condition at the chamber inlet, and the air carrier stream was employed as a velocity boundary condition. In the simulation configuration, the pressure pulse was applied via a user-defined function of a trapezoid pulse of 8 μs (2–10 μs with 1 μs rising/falling time) at the pressure inlet boundary (Fig. 4).

2.2 Numerical simulation using the VOF method

In this study, the simulation was performed using FLUENT 6.3. The simulation system was based on the solution algorithm scheme for the governing equations of the flow field, and the VOF method was adopted to capture the fluid interfaces. The surface tension was modeled using a CSF concept, and thus computed as a function of the interfacial curvature. This way the droplet ejection as well as phenomena occurring during droplet breakup due to the surface tension could be simulated and examined, providing the main advantage of the use of CFD simulations in descriptions of droplet deviation phenomena. According to the jetting system setup, a 3D mesh of the computational domain was created with emphasis placed on the outer part of the nozzle in Gambit 2.3.16 (Fig. 5).

The mesh of the nozzle part was symmetric (Fig. 5a). When meshing the outlet domain with the symmetric inlet face as the standard using quadrate/triangular facets, it is inevitable that asymmetric meshes are generated due to the inherent minimum volume loss principle of the software. Thus, asymmetry exists only in the outlet domain; the fluid motion, pressure propagation and interaction in the nozzle are actually under symmetric conditions. The minimum mesh size of 2 μm was chosen to attenuate the minute effect of asymmetry in local parts of outer domain. The details of the grid of the computational domain are listed in Table 1.

In the VOF method, the tracking of interfaces between fluid phases and multiple immiscible fluids are simulated by solving continuity, momentum, and volume fraction equations. Two phases were defined for the simulation: the primary phase was the continuous surrounding air, and the secondary phase was the discrete phase, the ejected ink. As most commercial inks are water-based, we simply chose water-liquid as the secondary phase material here. The properties of the phases used in the simulation are listed in Table 2.

For computational stability, an implicit algorithm was used in this study to solve the governing equations, and the k-epsilon (two-equation) model was chosen for the 3D pressure based time-dependent

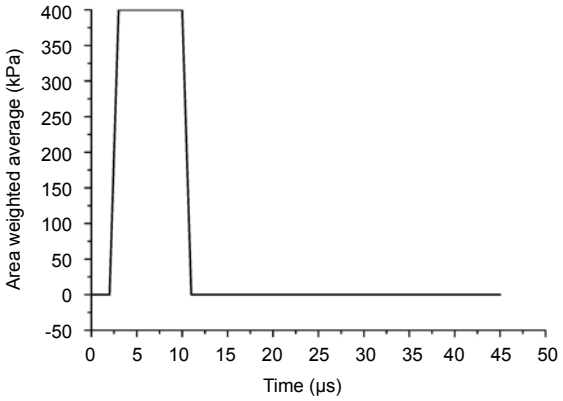

Fig. 4 Pressure wave applied as the initial condition in the simulation (400 kPa applied here)

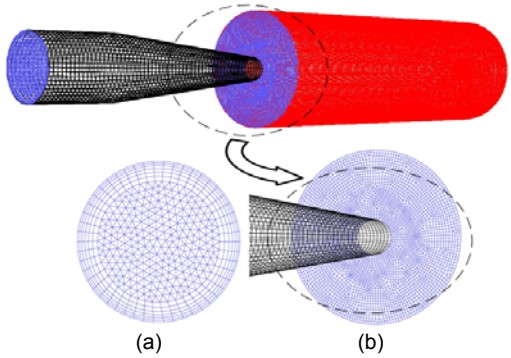

Fig. 5 3D mesh scheme of the computational domain
(a) Inlet 1: pressure inlet of ink chamber; (b) Inlet 2: velocity inlet of air carrier stream (v=0 m/s)

Table 1 Grid details of the computational domain

Parameter	Value	Parameter	Value
Cell number	716840	Node number	686698
Face number	2078107	Minimum grid	2 μm

Table 2 Properties of the two defined phases

Phase	Density (kg/m^3)	Viscosity (Pa·s)	Surface tension coefficient (N/m)
Air	1.225	1.7894×10^{-5}	0.073
Water	998.2	0.001	

solver. The algorithm adopted a second order upwind scheme, and non-iterative time advancement was implemented based on a sensitivity test. The geometric reconstruction scheme was also adopted to represent the interface between fluids using a piecewise linear approach. To satisfy the convergence requirement, the time step was taken as 0.1 μs, also based on a sensitivity test. With this framework, VOF copes with the loss of fluid volume by monitoring the convergence and computational residual errors of the governing equations by each iteration. The tolerance of the continuity equation was set as 1×10^{-6} in the simulations to keep computational error under an extremely low lever while the simulation parameters and conditions change.

3 Companion drops phenomena

A series of simulations was performed under different operating conditions using FLUENT 6.3. Fig. 6 illustrates two simulation sequences of droplet formation process under different excitation pressures. The droplet does not deviate from the central axis during the jetting process (Fig. 6a). However, as a few tiny drops break off from the main droplet at the initial stage of the ejection process (0–100 μs), droplet deviation occurs, and both the position and velocity of the droplet drift away from the central flying axis (Fig. 6b). In line with other simulation results, we conclude that the generation of these tiny drops will result in deviation of the main droplet. Accompanying the breaking-off of these tiny drops, the main droplet drifts away from the central jetting axis, bringing both positional and directional deviation perpendicular to the expected jetting direction.

In this study, we denote these tiny drops as "companion drops". Their generation accompanies the formation of the main droplet and droplet deviation. The features of companion drops are summarized below in comparison with those of satellite drops:

1. Satellite drops result from breakup of the ligament or "tail" of the ejected ink drop, while companion drops break off from the liquid surface of the main droplet. Accordingly, satellite separation occurs back behind the main droplet, companion drops generally break off from the front and sides of the main droplet.

2. Companion drops form almost synchronously as the droplet is being ejected out of the nozzle, typically, within the first 0–100 μs of the droplet

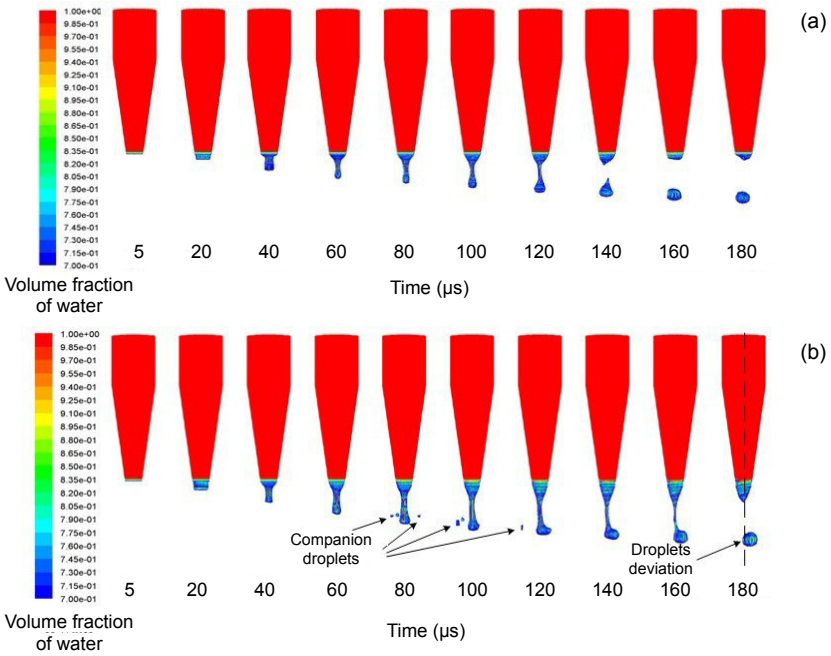

Fig. 6 Two simulation sequences of the droplet formation process

(a) Simulation sequence of droplet formation during ejection at 150 kPa: no droplet deviation occurs; (b) Simulation sequence of droplet formation during ejection at 250 kPa: droplet deviation occurs as some tiny imperceptible drops (companion drops) are generated

formation process, ahead of the generation of satellite drops, which generate during the flight period of the main droplet.

3. Satellite drops result in velocity change along the jetting direction and vertical to the printing medium, causing fight time and pattern distortion and ultimately placement errors indirectly due to the relative motion of the printing substrate. In contrast, companion drops cause mainly velocity and directionality deviation perpendicular to the flight axis and jetting direction, thus jeopardizing jetting straightness and printing accuracy more directly and acutely.

4. Considering the scale of these simulation sequences, the volumes of companion drops are quite small compared with satellite drops. Along with the randomness of their generation, companion drops are more difficult to capture with CCD cameras and study via experimental methods than are satellite drops.

4 Companion drops formation

4.1 Generation mechanism of companion drops

In this subsection we present a theoretical mechanism of companion drop generation. To simplify the theoretical modeling process, several assumptions have been made: (1) the fluid is Newtonian and incompressible, (2) the diffusion between the ambient environment and the fluid is negligible, and (3) the effects of gravity are negligible. With these characteristics, the continuity equation and Navier-Stokes equations governing the liquid motion are given in cylindrical, axisymmetric coordinates (r, z) as

$$\frac{\partial u}{\partial z}+\frac{1}{r}\frac{\partial (rv)}{\partial r}=0, \tag{1}$$

$$\rho\left(\frac{\partial v}{\partial t}+v\frac{\partial v}{\partial r}+u\frac{\partial v}{\partial z}\right)=\mu\left[\frac{\partial}{\partial r}\left(\frac{1}{r}\frac{\partial (rv)}{\partial r}\right)+\frac{\partial^2 v}{\partial z^2}\right]+\frac{\partial F_{\mathrm{b}}}{\partial r}-\frac{\partial P}{\partial r}, \tag{2}$$

$$\rho\left(\frac{\partial u}{\partial t}+v\frac{\partial u}{\partial r}+u\frac{\partial u}{\partial z}\right)=\mu\left[\frac{1}{r}\frac{\partial}{\partial r}\left(r\frac{\partial u}{\partial r}\right)+\frac{\partial^2 u}{\partial z^2}\right]+\frac{\partial F_{\mathrm{b}}}{\partial z}-\frac{\partial P}{\partial z}, \tag{3}$$

where u and v are the axial and radial components of the velocity field, respectively, P is the fluid pressure, μ is the fluid viscosity, and F_{b} is the volume force dominated mainly by surface tension. Based on the CSF mode of Brackbill *et al*. (1992), the volume force F_{b} can be translated as a continuous effect of surface tension across an interface and be computed using the following equation (Lai *et al*., 2010):

$$F_{\mathrm{b}}=f_\sigma\delta_\sigma, \tag{4}$$

where f_σ is the surface tension force per unit interfacial area, and δ_σ is a surface delta function restricting the surface tension force F_{b} being applied in the minute bounded region containing the interface. The fluid flow rate Q can be defined as

$$\frac{\partial Q}{\partial r}=ur, \text{ and } \frac{\partial Q}{\partial z}=-vr. \tag{5}$$

Considering Eqs. (5) and (1) together, the steam function can be written as

$$\frac{\partial^2 Q}{\partial z^2}+r\frac{\partial}{\partial r}\left(\frac{1}{r}\frac{\partial Q}{\partial r}\right)=r\left(\frac{\partial u}{\partial r}-\frac{\partial v}{\partial z}\right). \tag{6}$$

The jet configuration and reference frame of droplet formation from an ink-jet nozzle is illustrated in Fig. 7. As the liquid is being ejected out of the nozzle, a normal stress or pressure jump is generated at the surface relative to ambient gas pressure. The required surface pressure conditions in the local (τ, η) frames can be given as indicated (Fromm, 1984):

$$\frac{P}{\rho}-\left(\frac{P}{\rho}\right)_{\mathrm{air}}=\frac{\sigma}{\rho}\left(\frac{\cos\alpha}{r}-\frac{\partial\alpha}{\partial\tau}\right)+\frac{2\mu}{\rho}\left(\frac{\partial u_\eta}{\partial\eta}+u_\tau\frac{\partial\alpha}{\partial\eta}\right), \tag{7}$$

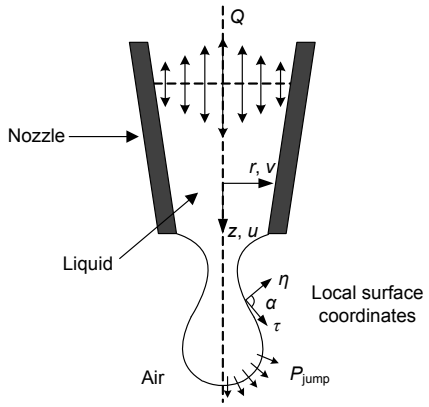

Fig. 7 Schematic of jet configuration and reference frame

where $u_\eta = -\frac{1}{r}\frac{\partial Q}{\partial \tau}$ and $u_\tau = \frac{1}{r}\frac{\partial Q}{\partial \eta}$ are the normal and tangential ejection velocities with respect to the local surface coordinates, respectively, P and ρ are the internal pressure and density of the liquid, respectively, and σ is the surface tension coefficient. Here $\frac{\partial \alpha}{\partial \tau}$ is the surface curvature or variation of the angle of the tangent to the interface; $\frac{\cos\alpha}{r}$ is the curvature about the axis of symmetry. Thus, the pressure jump at P_{jump} at the local liquid-air interface can be calculated using the relations given in Eq. (7) as

$$P_{\text{jump}} = P - P_{\text{air}} = \left(\frac{\rho}{\rho_{\text{air}}} - 1\right) P_{\text{air}} + \sigma\left(\frac{\cos\alpha}{r} - \frac{\partial \alpha}{\partial \tau}\right) + 2\mu\left(\frac{\partial u_\eta}{\partial \eta} + u_\tau \frac{\partial \alpha}{\partial \eta}\right). \tag{8}$$

Clearly, with α known for each surface point P_{jump}, the effects of curvature upon the pressure differential at the surface can be calculated. Thus, the generation mechanism of companion drops can be explained from Eqs. (7) and (8): if the value of P_{jump} at local parts of the liquid-air interface overcomes the constraint of volume force F_{b}, a certain volume of liquid will break off from the liquid surface, emerge into the air phase and generate companion drops. Furthermore, according to Xu and Basaran (2007), the interfacial pressure gradient reaches a maximum at the tips of the pendant droplet. Thus, the largest pressure jump is generated at the tip or frontal surface of the ejected liquid, making companion drops typically more prone to break off and form in these parts ahead of the main jet during ejection, as the simulation result shows.

4.2 Effects and behavior of companion drops

The generation of companion drops depends on the relative conditions between the interfacial pressure jump P_{jump} and the volume force dominated by surface tension. Once formed, companion drops will interact with the main droplet instantaneously. Generally, companion drops make an impact on the main droplet through two means: (a) The break-offs from companion drops have the major impact, forcing the main droplet to reshape under the volume force and to deviate from the expected jetting direction due to internal pressure perturbation and shape fluctuation. (b) The generation of companion drops introduces a momentum transfer with the main droplet, leaving a velocity component contrary to the main droplet, which also contributes to droplet deviation.

As the volume of a companion drop is much smaller than that of the main droplet, and its break off and interaction with the main droplet is instantaneous, its behavior is random and quite unpredictable. Generally, one of three phenomena may occur when companion drops break off from a main droplet: spreading around, merging or flying off. After break-offs, some companion drops keep on dispersing because of residual pressure turbulence, spreading around and finally fading away. In other cases, due to the tiny volume, the negligible gravity and the finite drag on these drops, some companion drops may seem to be "floating" in the air phase. As the ejection and expansion of the main droplet, some of these companion drops ahead of, or close to, the main droplet may merge into the liquid again, resulting in a recombination and second series of interactions. The remaining distant companion drops will ultimately fly away from the main droplet after a short period of shape fluctuation, leaving the main droplet with a contrary velocity and significant deviation. All of these behaviors are undesirable in most circumstances and inkjet applications.

Fig. 8 shows the sequence of main droplet formation accompanied by companion drops under an inlet pressure of 450 kPa. All three behaviors of companion drops as discussed above can be observed. As a relative high pressure pulse (450 kPa) is applied at the nozzle entrance, the break-off area at the liquid surface expands from certain local facets of the liquid tip to the semicircular zone at the front of the ejected liquid. Companion drops may even burst into a mist of ink around the main droplet, which may ultimately cause tiny undesirable spots on the printing medium as well as poor printing quality or even printing failure.

5 Influencing factors

The ink jetting and droplet formation process is sensitive to several factors, including waveform, nozzle structure and liquid properties (Eslamian and Ashgriz, 2011). Table 3 shows the physical properties

and printable ranges (p_l–p_u) of water and a water-based commercial ink implemented by the jetting system in Section 1, where the lower bound p_l is the minimum inlet pressure at the chamber entrance sufficient for the creation of a drop, and the upper bound p_u is the inlet threshold pressure below which a single droplet is ejected and well formed without companion drops and droplet deviation. In this study, the printable pressure range was chosen as an indicator to characterize companion drops formation.

The printable range is actually narrow, especially for ink with lower surface tension (Table 3). In modern ink jetting applications, the pressure pulse plays an important role in the parametric control of droplet velocity and volume in the ejection process. A narrow and improper printable range places restrictions on the droplet velocity, volume and other jetting parameters, ultimately limiting the ink jetting operating conditions, while a wide and stable printable range provides an ideal foundation for ink jetting control and printing performance improvement. For the purpose of droplet deviation suppression and printable range regulation, the effects of factors related to the formation of companion droplets were further investigated through numerical simulations.

5.1 Effects of the excitation pulse width

The inkjet waveform used to excite a piezoelectric transducer can significantly alter jetting behavior (Kim *et al*., 2005). Dong *et al*. (2006) showed that satellite behavior could be changed by modifying the driving waveform. Shin *et al*. (2011) applied double waveforms with two square pulses to control the droplet formation in a piezoelectric inkjet nozzle and its response was investigated. Lai and Lin (2010) investigated the effect of the component of a single transducer pulse on the ejection of a drop for a piezoelectric printhead through numerical calculations. Kwon (2009) proved that it is possible to obtain the optimal condition for stable drop formation by tuning the pulse width.

To explore the effect of pulse width on companion drops, pressure pulses with gradient widths from 2 μs to 16 μs in time increments of 2 μs were applied in a series of numerical simulations, and the variation in printable range determined (Fig. 9). With increasing pulse width, the printable pressure range narrows down as both the bounds p_u and p_l decrease exponentially.

This variation can be explained simply from the view of energy transfer. In a DOD jetting system, the energy generated by a piezo actuator is transferred as a pressure wave propagating in the liquid towards the

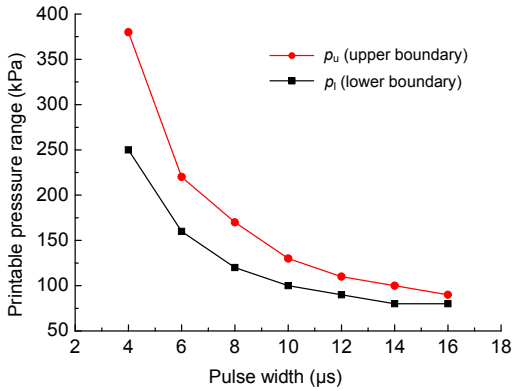

Fig. 9 Variation of the printable pressure range as a function of pulse width

Table 3 Printable ranges of water and a commercial ink (Link and Semiat, 2009)

Phase	Density (kg/m^3)	Viscosity (Pa·s)	Surface tension (N/m)	p_l (kPa)	p_u (kPa)
Water	998.2	0.001	0.073	120	170
Ink	999.5	0.01003	0.039	140	180

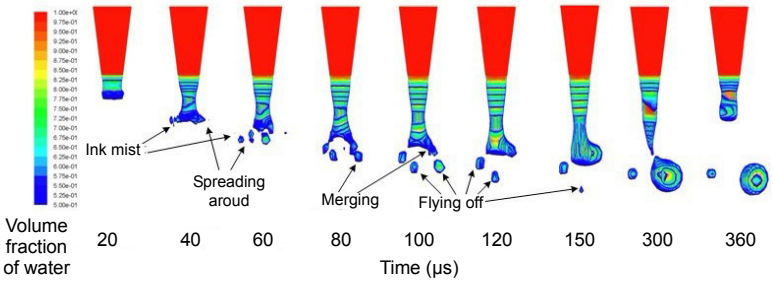

Fig. 8 Droplet formation at 450 kPa with generation of companion drops and droplet deviation

orifice at the nozzle end. The larger is the pulse width, the greater is the energy contained in the wave, and the pressure turbulence that the wave brings to the interface of the liquid after its propagation and decay. In theory, a larger pulse width brings longer acceleration and consequently greater velocity and momentum to the ejected liquid, which increases the ejection velocity and the velocity term $\frac{\partial u_\eta}{\partial \eta}+u_\tau\frac{\partial \alpha}{\partial \eta}$ in Eq. (8), causing a larger pressure jump at the liquid-air interface. Once the pressure turbulence/jump overwhelms the volume force, companion drops will break off, resulting in undesirable droplet deviation. Thus, a larger width of the excitation pulse promotes the break-off and generation of companion drops. Hence, properly shortening the pulse width is a wise operation for stable droplet formation without companion drops.

5.2 Effects of nozzle geometry

Nozzle geometry is another factor critical to the ink jetting process. As the pressure wave propagates in the nozzle, the pressure magnitude decreases due to geometric resistance and reflection. The geometry of the nozzle has significant impacts upon the acoustic impedance, travel time of the pressure wave given by the channel length, the phase shift of the reflected wave, and the effective speed of sound inside the channel. In previous studies, the effects of nozzle geometry and liquid hydrophobicity were investigated and suggestions were made for defining an empirical nozzle design (Lai *et al*., 2010). The influence of the geometry on the stability of both the tapering liquid meniscus and the emitted jet was investigated and analyzed experimentally (Yobas *et al*., 2006; Vega *et al*., 2010). Here, we describe the influences of the orifice diameter, nozzle length and taper on the printable range through numerical simulations.

Figs. 10 and 11 are respectively the variations in the printable pressure range with different diameters of nozzle orifice and lengths of the nozzle taper. As the nozzle diameter and the length of the nozzle taper increase successively, the printable pressure range rises almost linearly. But the increments of the range bounds p_u and p_l are nearly synchronous and equivalent, thereby restricting expansion of the width of the printable pressure range which remains almost unchanged at about 50 kPa. The geometry of the nozzle influences droplet formation mainly through its impact on the wave impedance, which has a homogeneous effect on the wave propagation in the liquid. Nozzle geometry also influences the shape and curvature of the ejected liquid, which slightly affects the pressure jump at the surface according to Eq. (8). Carefully tuning the parameters of nozzle geometry, and adjusting the printable range according to the operating conditions of the printhead, help to suppress companion drops and achieve better printability.

5.3 Effects of liquid properties

As liquid properties are involved in several critical events, such as the transference of the pressure wave, ejection and interaction of the ink thread, and formation and behavior of ink droplets, it is essential to understand clearly how the liquid properties affect jetting stability, namely, the generation of companion drops. To investigate the effects of jetting material properties, important parameters of fluids are

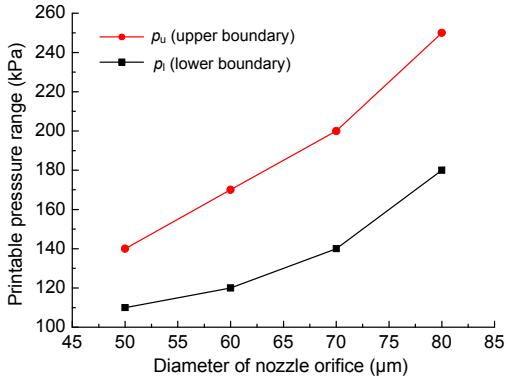

Fig. 10 Variation in the printable pressure range as a function of nozzle diameter

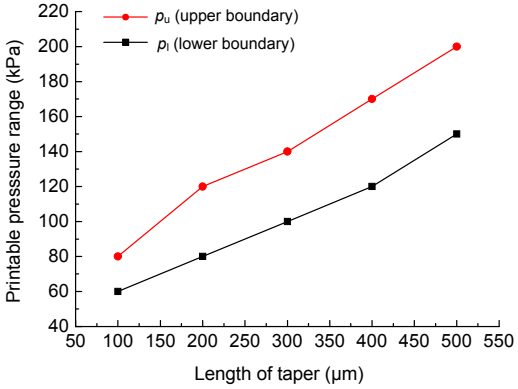

Fig. 11 Variation in the printable pressure range as a function of taper length of the nozzle

characterized typically by the inverse (Z) of the Ohnesorge number (Oh), which is defined as follows:

$$Z=\frac{(a\rho\sigma)^{1/2}}{\mu}, \tag{9}$$

where ρ, σ, μ and a are the density, surface tension and viscosity of the fluid and the radius of the nozzle orifice, respectively. Correlations between the drop formation process and the physical characteristics of the fluid were analyzed during previous experimental and numerical research. Jang *et al*. (2005) investigated the inter-relationship between ink-jet printability and physical fluid properties, and determined the printable range as $4\leq Z\leq 14$ by monitoring droplet formation dynamics. Reis *et al*. (2005) proposed that a higher Z value results in a more pronounced satellite in the jetted droplet. In this study, the correlations between the printable range and the Z number were explored using five glycerol-water solutions with different glycerol volume percentages. The material properties of the glycerol-water solutions are shown in Table 4. The change in glycerol volume percentage directly alters the viscosity, surface tension, density, and Z numbers of the glycerol solutions.

Fig. 12 shows the variation in printable pressure range as a function of Z numbers. For $Z<20$, p_u and p_l decrease exponentially, and the printable range narrows down sharply as the Z value increases. For $Z>20$, variation in p_u and p_l is not distinctive, and the printable range remains almost stationary as 120–170 kPa accordingly. Generally, companion drops tend to break off and generate more easily when liquids with higher Z values are used. This is a comprehensive result due to the complicated and even conflicting effects of the factors involved: (1) The larger liquid density ρ denotes a larger pressure jump according to Eq. (8), while larger liquid density reduces the ejection velocity and the velocity term $\frac{\partial u_\eta}{\partial \eta}+u_\tau\frac{\partial \alpha}{\partial \eta}$ to a fixed momentum. (2) Viscosity denotes the impedance of the fluid to the acoustic wave. A higher viscosity indicates a larger viscous force and a larger damping effect on the momentum of the ejected liquid, thereby suppressing the pressure jump at the liquid-air surface. However, a higher viscosity indicates a larger pressure jump term $2\mu\left(\frac{\partial u_\eta}{\partial \eta}+u_\tau\frac{\partial \alpha}{\partial \eta}\right)$ in Eq. (8). (3) The surface tension σ denotes the conflicting volume force in Eq. (4) and the term $\sigma\left(\frac{\cos\alpha}{r}-\frac{\partial \alpha}{\partial \tau}\right)$ in Eq. (8) at the same time. All these coupled factors combine to make an integrated impact on the ejection process and companion drop generation, resulting in compromise effects in different aspects.

5.4 Effects of surface tension

In Table 4, the glycerol-water solutions have almost the same static surface tension, which is a little lower than that of deionized water. However, according to Eq. (4), surface tension plays an important role in the generation of companion drops owing to its dominant effect on the volume force. A higher surface tension indicates a larger volume force, increasing the jetting stability to pressure jump or turbulence at the liquid interface. However, considering Eq. (8), a higher surface tension may result in larger term of $\sigma\left(\frac{\cos\alpha}{r}-\frac{\partial \alpha}{\partial \tau}\right)$ for higher pressure jump, which

Table 4 Physical properties and Z numbers of the glycerol-water solutions

Glycerol volume percentage (%)	Density (kg/m^3)	Surface tension (mN/m)	Viscosity (mPa·s)	Z number
0	998.2	73.5	1	46.915 15
10	1029.1	70.3	1.26	36.974 01
20	1059.5	69.1	1.8	26.036 2
30	1088.6	68.2	2.71	17.414 77
40	1116.1	67.6	4.28	11.115 83
50	1142.5	67.1	7.33	6.542 534

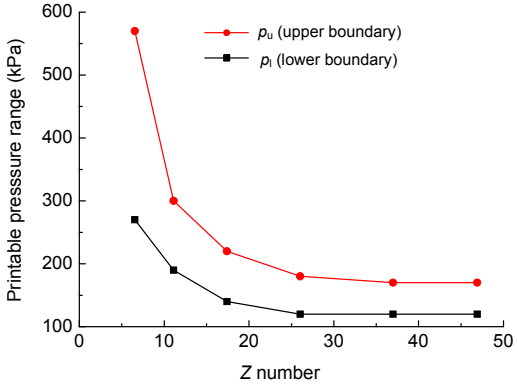

Fig. 12 Variation in the printable pressure range as a function of the Z number

promotes the generation of companion drops. To investigate these two conflicting effects, an extra series of simulations was carried out with surface tension as variable and other properties set hypothetically as constants (water-liquid: viscosity of 0.001 Pa·s, density of 998.2 kg/m^3). Fig. 13 illustrates the variation in printable pressure range as a function of surface tension coefficient.

The printable pressure range rises and expands almost linearly as the surface tension coefficient increases (Fig. 13). Also, several offsets occur in the variation lines due to the effects of surface tension on the pressure jump. Generally, surface tension influences the printable range primarily through its major role in determining the volume force, and a higher surface tension indicates a wider pressure range. For most commercial water-based inks, whose physical properties are similar to those of water-liquid except for the surface tension coefficient, the choice of inks with a high surface tension should improve the printable range and printability.

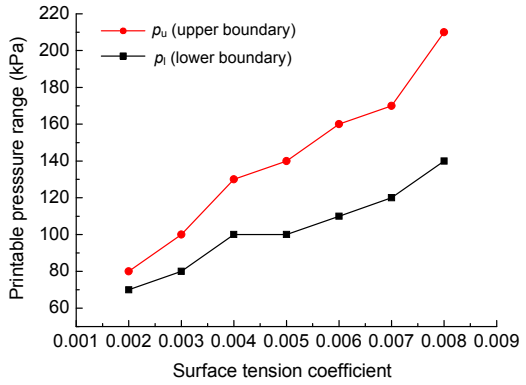

Fig. 13 Variation in the printable pressure range as a function of surface tension coefficient

6 Conclusions

In this paper, we presented the investigation and characterization of the specific phenomena of companion drops by coupling computational simulations with theoretical analysis. Major conclusions are summarized as follows.

1. The formation of companion drops is a critical phenomenon that causes droplet deviation, which is closely correlated with ink jetting performance and printing accuracy. In contrast to satellite drops, companion drops break off from the tips or frontal facets of the liquid surface at the initial stage, typically in the first 0–100 μs of the ejection process, causing velocity drift perpendicular to the flight axis and deviation from the expected jetting direction, thereby jeopardizing jetting straightness and reducing printing accuracy directly and intensively.

2. The generation of companion drops is governed by the pressure jump P_{jump} at the surface of ejected liquid relative to ambient gas pressure and depends on the interaction between the pressure jump P_{jump} and the constraint of volume force F_{b}. Specifically, once the pressure jump at the liquid-air interface overwhelms the volume force in local parts of the liquid-air interface, companion drops will break off from the ejected liquid, bringing pressure perturbation, shape fluctuation and ultimately undesirable deviation to the main droplet.

3. The effects of critical factors involved in the generation of companion drops were investigated and characterized using the printable pressure range as an indicator of printability. Proper shortening of the excitation pulse width, careful tuning of the geometry of the nozzle, and choosing liquids with smaller Z values or higher surface tensions, help to tune and expand the printable pressure range and suppress the generation of companion drops.

Currently, there is no experimental proof of the existence of these companion drops, thus we plan to construct a feasible experimental scheme to validate and complement our findings in this paper, and to investigate this issue further.

References

Anantharamaiah, N., Tafreshi, H.V., Pourdeyhimi, B., 2007. A simple expression for predicting the inlet roundness of micro-nozzles. *Journal of Micromechanics and Microengineering*, **17**(5):N31-N39. [doi:10.1088/0960-1317/17/5/N01]

Brackbill, J.U., Kothe, D.B., Zemach, C., 1992. A continuum method for modeling surface-tension. *Journal of Computational Physics*, **100**(2):335-354. [doi:10.1016/0021-9991(92)90240-Y]

Cibis, D., Krüger, K., 2008. Optimization of a DOD Print Head Signal for the Ink-Jetting of Conductive Circuits. International Conference on Non-Impact Printing, NIP24, Pittsburgh, USA, p.125-128.

Dijksman, J.F., Duineveld, P.C., Hack, M.J.J., Pierik, A., Rensen, J., Rubingh, J.E., Schram, I., Vernhout, M.M., 2007. Precision ink jet printing of polymer light emitting

displays. *Journal of Materials Chemistry*, **17**(6):511-522. [doi:10.1039/b609204g]

Dong, H., Carr, W.W., 2006. An experimental study of drop-on-demand drop formation. *Physics of Fluids*, **18**(7): 072102. [doi:10.1063/1.2217929]

Dong, H., Carr, W.W., Morris, J.F., 2006. Visualization of drop-on-demand inkjet: drop formation and deposition. *Review of Scientific Instruments*, **77**(8):085101. [doi:10.1063/1.2234853]

Eslamian, M., Ashgriz, N., 2011. Drop-on-Demand Drop Generators. Handbook of Atomization and Sprays, Part 3, p.581-601. [doi:10.1007/978-1-4419-7264-4_25]

Fromm, J.E., 1984. Numerical calculation of the fluid dynamics of drop-on-demand jets. *IBM Journal of Research and Development*, **28**(3):322-333. [doi:10.1147/rd.283.0322]

Goghari, A., Chandra, S., 2007. Producing droplets smaller than the nozzle diameter by using a pneumatic drop-on-demand droplet generator. *Experiments in Fluids*, **44**(1): 105-114. [doi:10.1007/s00348-007-0378-z]

Hoath, S.D., Hutchings, I.M., Martin, G.D., Tuladhar, T.R., Mackley, M.R., Vadillo, D., 2009. Links between ink rheology, drop-on-demand jet formation, and printability. *Journal of Imaging Science and Technology*, **53**(4): 041208. [doi:10.2352/J.ImagingSci.Technol.2009.53.4.041208]

Jang, D., Kim, D., Moon, J., 2009. Influence of fluid physical properties on ink-jet printability. *Langmuir*, **25**(5):2629-2635. [doi:10.1021/la900059m]

Kim, M.K., Kang, H.S., Kang, K.T., Cho, Y.J., Park, M.S., Kim, Y.J., 2005. The Fluid Property Dependency on Ink Jetting Characteristics. Proc. IEEE Int. Conf. on Mechatronics, Taiwan, Taipei, p.258-260. [doi:10.1109/ICMECH.2005.1529264]

Kwon, K.S., 2009. Waveform design methods for piezo inkjet dispensers based on measured meniscus motion. *Journal of Microelectromechanical Systems*, **18**(5):1118-1125. [doi:10.1109/JMEMS.2009.2026465]

Kwon, K.S., 2010. Experimental analysis of waveform effects on satellite and ligament behavior via in situ measurement of the drop-on-demand drop formation curve and the instantaneous jetting speed curve. *Journal of Micromechanics and Microengineering*, **20**(11):115005. [doi:10.1088/0960-1317/20/11/115005]

Lai, J.M., Lin, J.D., 2010. Numerical investigation of the effect of a transducer pulse on the microfluidic control of a piezoelectric printhead. *Journal of Micro/Nanolithography, MEMS, and MOEMS*, **9**(3):033010. [doi:10.1117/1.3486201]

Lai, J.M., Huang, C.Y., Chen, C.H., Kung, L., Lin, J.D., 2010. Influence of liquid hydrophobicity and nozzle passage curvature on microfluidic dynamics in a drop ejection process. *Journal of Micromechanics and Microengineering*, **20**(1):015033. [doi:10.1088/0960-1317/20/1/015033]

Link, N., Semiat, R., 2009. Ink drop motion in wide-format printers I. Drop flow from drop-on-demand (DOD) printing heads. *Chemical Engineering and Processing: Process Intensification*, **48**(1):68-83. [doi:10.1016/j.cep.2008.02.005]

Moon, K.S., Choi, J.H., Choi, D.J., Kim, S.H., Ha, M.H., Nam, H.J., Kim, M.S., 2008. A new method for analyzing the refill process and fabrication of a piezoelectric inkjet printing head for LCD color filter manufacturing. *Journal of Micromechanics and Microengineering*, **18**(12): 125011. [doi:10.1088/0960-1317/18/12/125011]

Notz, P.K., Chen, A.U., Osman, A.B., 2001. Satellite drops: unexpected dynamics and change of scaling during pinch-off. *Physics of Fluids*, **13**(3):549-552. [doi:10.1063/1.1343906]

Reis, N., Ainsley, C., Derby, B., 2005. Ink-jet delivery of particle suspensions by piezoelectric droplet ejectors. *Journal of Applied Physics*, **97**(9):094903. [doi:10.1063/1.1888026]

Shin, P., Sung, J., Lee, M.H., 2011. Control of droplet formation for low viscosity fluid by double waveforms applied to a piezoelectric inkjet nozzle. *Microelectronics Reliability*, **51**(4):797-804. [doi:10.1016/j.microrel.2010.11.017]

Suh, Y., Son, G., 2008. A level-set method for simulation of a thermal inkjet process. *Numerical Heat Transfer Part B: Fundamentals*, **54**:138-156. [doi:10.1080/10407790802182661]

Vega, E.J., Montanero, J.M., Herrada, M.A., Gañán-Calvo, A.M., 2010. Global and local instability of flow focusing: The influence of the geometry. *Physics of Fluids*, **22**(6): 064105. [doi:10.1063/1.3450321]

Wijshoff, H., 2010. The dynamics of the piezo inkjet printhead operation. *Physics Reports*, **491**(4-5):77-177. [doi:10.1016/j.physrep.2010.03.003]

Wu, H.C., Hwang, W.S., Lin, H.J., 2004. Development of a three-dimensional simulation system for micro-inkjet and its experimental verification. *Materials Science and Engineering: A*, **373**(1-2):268-278. [doi:10.1016/j.msea.2004.01.043]

Xu, Q., Basaran, O.A., 2007. Computational analysis of drop-on-demand drop formation. *Physics of Fluids*, **19**(10): 102111. [doi:10.1063/1.2800784]

Yobas, L., Martens, S., Onga, W., Ranganathan, N., 2006. High-performance flow-focusing geometry for spontaneous generation of monodispersed droplets. *Lab on a Chip*, **6**(8):1073-1079. [doi:10.1039/b602240e]

Yu, J.D., Sakai, S., Sethian, J., 2005. A coupled quadrilateral grid level set projection method applied to ink jet simulation. *Journal of Computational Physics*, **206**:227-251. [doi:10.1016/j.jcp.2004.12.012]